The Journal of Chemical Physics

A soft x-ray probe of a titania photoelectrode sensitized with a triphenylamine dye

Cite as: J. Chem. Phys. **154**, 234707 (2021); https://doi.org/10.1063/5.0050531
Submitted: 16 March 2021 . Accepted: 28 May 2021 . Published Online: 17 June 2021

Robert H. Temperton, Jack Hart, Nektarios Verykokkos, Elizabeth Gibson, and James N. O'Shea

The Journal of Chemical Physics ARTICLE scitation.org/journal/jcp

A soft x-ray probe of a titania photoelectrode sensitized with a triphenylamine dye

Cite as: J. Chem. Phys. 154, 234707 (2021); doi: 10.1063/5.0050531
Submitted: 16 March 2021 • Accepted: 28 May 2021 •
Published Online: 17 June 2021

Robert H. Temperton,[1,a)] Jack Hart,[2] Nektarios Verykokkos,[3] Elizabeth Gibson,[3] and James N. O'Shea[2,a)]

AFFILIATIONS

[1] MAX IV Laboratory, Lund University, Box 118, 221 00 Lund, Sweden
[2] School of Physics and Astronomy, University of Nottingham, University Park, Nottingham NG7 2RD, United Kingdom
[3] Energy Materials Laboratory, Chemistry, School of Natural and Environmental Science, Newcastle University, Newcastle upon Tyne NE1 7RU, United Kingdom

[a)] **Authors to whom correspondence should be addressed:** robert.temperton@maxiv.lu.se and J.Oshea@nottingham.ac.uk

ABSTRACT

We present a thorough soft x-ray photoelectron spectroscopy (XPS) study of a mesoporous titanium dioxide electrode sensitized with the dye 4-(diphenylamino)phenylcyanoacrylic acid, referred to as "L0." Supported by calculations, the suite of XPS, x-ray absorption spectroscopy, and resonant photoelectron spectroscopy allows us to examine bonding interactions between the dye and the surface and the frontier electronic structure at the molecule–oxide interface. While placing these measurements in the context of existing literature, this paper is intended as a useful reference for further studies of more complex triphenylamine based sensitizers.

I. INTRODUCTION

Solar energy conversion remains highly topical, and despite the prevalence of silicon solar cells, the use of organic systems for light harvesting remains of interest for a range of sustainable next generation devices.[1–5] One of the most studied molecular approaches is the dye sensitized solar cells (DSCCs),[6] the operating principle of which relies on ultra-fast electron injection from a photoexcited dye molecule into a semiconductor surface.[4] However, approaching 20 years after the advent of the now ubiquitous "Grätzel cell" with 7% efficiency,[7] many of the limitations of DSSCs have yet to be overcome, including their stability and efficiency compared to competitive technologies.[3] Despite this, some advantages of DSSCs remain appealing, for example, they are semi-transparent and their absorption spectrum, i.e., color, can be tuned through the use of different dyes. Until recently, however, blue dyes have been largely absent from the available color pallet of viable DSSCs due to the absence of a low cost and high efficiency dye. Although several blue dyes have been announced in recent years,[8–11] perhaps the most exciting to date is "R6," which produced a blue DSSC with 12.6% efficiency.[12]

Understanding the fundamental properties of "R6" and related dyes is therefore of great interest, and synchrotron based photoelectron spectroscopy (PES) has proven to provide a powerful set of tools for studying bonding, charge transfer, and the molecular orbital structure of photofunctional molecules.[13–16] In order to apply photoelectron spectroscopy techniques to increasingly complex molecules, there is, of course, merit to first study the molecular building blocks before studying the complete molecule.[17] A common property of "R6" and the other blue dyes highlighted above is a triphenylamine type moiety, making the simpler "L0" dye, shown in Fig. 1, an ideal model system to study. As such, L0 and related small triphenylmethane based molecules have been the focus of some synchrotron[18–21] and computational[22,23] studies. Other investigations have examined molecules with longer ligands branching off the trimethylamine moiety.[24,25] This paper goes back to the basic L0 molecule and presents supporting and complimentary measurements while reviewing the highlights of this existing literature. We intend for this study to act as a step toward investigations of the flagship triphenylamine based sensitizers.

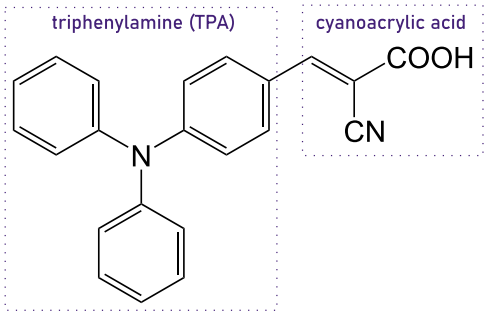

FIG. 1. Scheme of 4-(diphenylamino)phenylcyanoacrylic acid, referred to as "L0."

II. METHODS

A. Experimental

1. Sample preparation

Photoelectrodes were prepared by soaking mesoporous TiO_2 on fluorine-doped tin oxide (FTO) coated glass (from Solaronix) in a saturated solution of L0 (from Dyenamo AB) in acetonitrile for 12 h. They were then rinsed in acetonitrile before being left to soak for several hours in clean acetonitrile, which was repeated until the acetonitrile remained clear. This was carried out in a nitrogen atmosphere glove box (>0.1 ppm H_2O and O_2), and the samples were transferred under nitrogen to the beamline where they were exposed to air for >1 h before being transferred into vacuum.

2. Beamline and endstation

Measurements were taken at the Surface and Material Science (SMS) endstation on the FlexPES beamline at the MAX IV synchrotron radiation facility in Sweden. FlexPES, situated on the 1 GeV storage ring, uses a planar undulator and collimated plane-grating monochromator to deliver 40–1500 eV photons, which can be focused to a 65 × 10 μm spot at the SMS branch sample position or defocussed producing a larger size of 1.0 × 0.4 mm^2. The experimental station is equipped with a Scienta SES-2002 hemispherical analyzer for photoelectron spectroscopy (PES), positioned at an angle of 40° from the incident photon beam, and a home built partial electron yield (PEY) microchannel plate (MCP) detector for x-ray absorption measurements. Measurements were taken at normal emission where the sample pointed toward the analyzer.

3. Spectroscopy

PES was measured using a pass energy of 50 eV in swept mode, giving an overall theoretical resolution of 0.21 and 0.19 eV at 600 and 220 eV photon energies, respectively. Resonant photoelectron spectroscopy (RPES) maps were measured in fixed mode with a pass energy of 200 eV, where the resolution was 0.75 eV. N 1*s* (K-edge) NEXAFS was measured in both total electron yield (TEY) via the sample drain current and also using the partial electron yield (PEY) MCP detector with a retardation potential of 300 V to suppress the contribution of low energy electrons to the background. During these measurements, I_0 was simultaneously measured on an Au mesh in the beam path. Comparison of total and partial electron yields shows the spectra are very similar (comparison is included in the supplementary material), but the data presented in the manuscript is all partial yield as the higher photon energy resonances are slightly better resolved. The photon energy resolution was 50 meV at the N-K edge.

4. Radiation damage

These molecules were susceptible to radiation damage, which was most obvious in the N 1s (K-edge) NEXAFS (see the supplementary material). Beam damage was avoided by using a defocussed beam (increasing the x-ray spot size on the sample to ~ (1.3 × 0.4) mm (h × v, FWHM) and regularly moving the sample in the beam). In the case of the RPES map, every photon energy line was measured on a fresh molecule. NEXAFS was used to confirm that the data collected represents un-damaged molecule (see the supplementary material).

5. Energy calibration

Using x-ray photoelectron spectroscopy (XPS), measured at $h\nu$ = 600 eV, binding energy (BE) scales were calibrated by setting the Ti $2p_{3/2}$ peak to 458.80 eV. This value was determined by measurement of a bare electrode, where the O 1*s* was set to 530.05 eV[26] (data included in the supplementary material). Valence band spectra, measured at $h\nu$ = 220 eV, were calibrated back to the Ti $2p_{3/2}$ reference via the Ti 3*p* peaks. These calibration methods were accurate to within 0.1 eV. Photon energy scales and the repeatability of beamline energy were confirmed to be accurate to within 50 meV by measurement of the kinetic energy difference of photoemission peaks generated from first and second order light.

6. Data processing

XPS data were peak fitted using a pseudo-Voigt function allowing absolute control of the Lorentzian and Gaussian widths. For each spectra, the Lorentzian contribution was fixed across all components. The Gaussian widths were constrained to be equal for molecule features but allowed to vary from the surface peaks. A linear or Shirley background was subtracted prior to curve fitting. Details of these parameters can be found in the captions of the relevant figures. NEXAFS spectra were divided through by I_0 with no further processing applied. Every RPES scan was normalized to the intensity of the C 1*s* core level measured on the same spot after the RPES measurement was complete. As each photon energy was measured at a different sample position, this normalization compensated for any minor variations in sample inhomogeneity and variations in flux of the incident photons.

B. Computational

Density functional theory (DFT) calculations were performed using the Q-Chem 5.2 quantum chemistry software package.[27] The geometry of an isolated L0 molecule was optimized using the B3LYP exchange–correlation functional[28,29] and a 6-311G** basis set[30] with a SCF (self consistent field) convergence criterion of 10^{-8}. A single point energy calculation, alongside the supporting time dependent (TD)-DFT, was performed on this optimized structure using the second form of the short range corrected functional[31] (SRC2-R1 as implemented in Q-Chem) with the same basis set and SCF convergence criteria. The TD-DFT was a 100 root restricted space calculation allowing single excitations from the two N 1*s* orbitals to any of the virtual orbitals. Kohn–Sham molecular orbitals were plotted using the IQmol software package[32] using an isovalue of 0.04 $Å^{-3}$. The C 1*s* binding energies were estimated by simply taking the

negative value of the calculated orbital energies in accordance with Koopman's theorem, but we note this approach only considers the initial state.[33] These calculated C 1*s* energies were offset/calibrated such that the HOMO energy matched the experiment.

III. RESULTS AND DISCUSSION

The electrodes studied here are prepared *ex situ*. It is therefore important to preface the results with a brief discussion of contamination. XPS measurements of a bare TiO_2 electrode are included in the supplementary material. Of particular relevance are Figs. S2 and S3, which show wide area scans and individual core levels, respectively. The wide area scan shows that the levels of nitrogen and carbon contamination are low in the case of the bare electrode. The O 1*s* shows notable contribution of absorbed species on the titania, likely originating from absorbed H_2O and/or OH species. However, it is not possible to draw a direct link between any contaminants apparent on the bare electrodes and the L0 sensitized electrodes due to the solution processing of the L0 electrodes. It is possible that the solution processing displaces physisorbed contaminants and equally possible that new contaminants are introduced. While this is worthy of future study, it is not the focus of this manuscript. We will proceed under the assumption that the contribution of such contaminants is minor but discuss it where relevant.

A. Core-level spectroscopy

O 1*s* XPS of the L0 sensitized electrode is presented in Fig. 2 and is fitted with three components. The dominant feature at 530.0 eV is attributed to the oxide surface while the two components to higher binding energy are attributed to the C = O and C–OH environments in the molecule's carboxylic acid ligand. These two peaks, at 531.4 and 532.8 eV, respectively, have relative areas of 0.7 (C = O) and 0.3 (C–OH). These assignments and peak separations are consistent to previous measurements of L0[19] and other molecules with carboxylic acid ligands.[26,34]

The O 1*s* peak areas do not match the 1:1 ratio apparently in the molecular structure. This is attributed to deprotonation of the carboxyl (C–OH), consistent with the now well established bidentate bridging bonding interaction of carboxylic acid groups with titanium dioxide surfaces, where both oxygen atoms bond with the oxide.[35,36] Here, we would expect the C–O–Ti oxygen environment to be at a similar energy to C = O, as previously shown for the case of L0 absorbed on single crystal titania.[21] The presence of the C–OH feature indicates that not all the molecules present are bonded to the surface by this geometry. One explanation is some physisorbed molecules remaining in the sample, perhaps due to insufficient washing. Alternatively, it is possible that a proportion of the molecules are in a different bonding geometry. For carboxylic acids, the bidentate bridging geometry is energetically favorable over those that preserve the protonated OH, such as the monodentate geometry.[37] However, L0 is a cyanoacrylic acid where the –C ≡ N group opens up additional bonding possibilities. In the case of anatase surfaces, calculations show that, for the 001 surface, bidentate bridging through the carboxylic acid is energetically favorable, but for the 101 surface, the most stable geometry is the dissociated bidentate configuration where the bonding is through the –C ≡ N and –C = O groups.[38] In a mesoporous surface, a mix of 001 and 101 structures would not be surprising, so it is possible that the presence of the C–OH peak is evidence of this additional bonding geometry. Computational work specifically on L0 has, however, investigated the bonding geometry; in vacuum, a monodentate geometry is slightly favorable, but in solution, (as our samples were prepared) the bidendate geometry is favorable.[22,23]

Residual contamination of the titania is also a possibility. Absorbed species, such as hydroxyls, may contribute to the O 1*s* intensity if present. We have previously studied the adsorption of water on titania and found OH and H_2O to appear in the O 1*s* at 1.3 and 2.6 eV, respectively, relative to the surface oxide peak.[39] If present, these features would certainly impact the O 1*s* fitting presented.

Figure 3 shows N 1*s* XPS data, fitted with two components attributed to the nitrogen environments in the triphenylamine and nitrile (C ≡ N) moieties. These two peaks at binding energies of

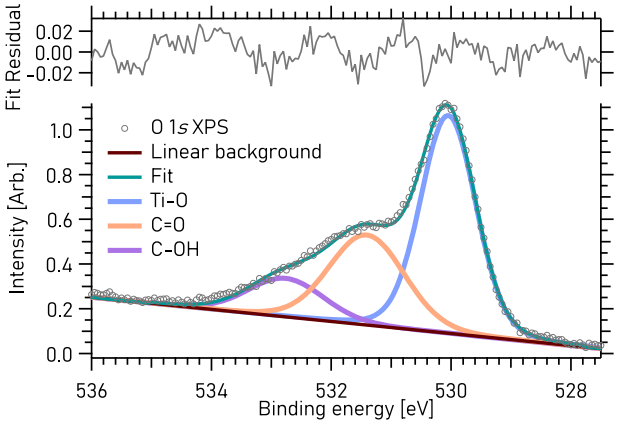

FIG. 2. O 1*s* spectrum, measured with 600 eV photons, fitted with components attributed to the titanium dioxide surface (blue) alongside the C = O (orange) and C–OH (purple) environments in the carboxylic acid ligand. All three peaks have a Lorentzian width of 0.1 eV. The titania and molecule features have Gaussian widths of 1.0 and 1.4 eV, respectively.

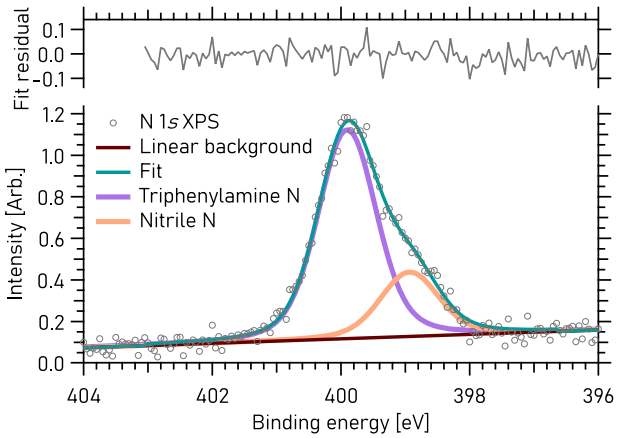

FIG. 3. N 1*s* spectrum, measured with 600 eV photons, fitted with components attributed nitrile [C≡N] and triphenylamine [$(C_6H_5)_3N$] nitrogen environments. Both peaks have a Lorentzian and Gaussian widths of 0.3 and 0.9 eV, respectively.

400.0 and 399.0 eV have normalized areas of 0.77 and 0.23, respectively, approximately with a 3:1 ratio. Our assignment and 1.0 eV peak separation are comparable with independent measurements of the same molecule,[20,21] similar molecules,[18,19] as well a study comparing N 1*s* binding energies of various nitrogen environments, including triphenylamine and nitrile.[40]

The N 1*s* data would initially appear inconsistent with the 1:1 ratio of nitrogen atoms in the triphenylamine and nitrile groups. However, if the molecule is anchored by the carboxylic acid ligand and oriented in an upright geometry, the triphenylamine end of the molecule will bury the nitrile group leading to a reduction in intensity. This effect on the nitrogen core level intensities has been explored with a very similar molecule on mesoporous TiO_2, where the surface sensitivity is controlled by varying the incident photon energy,[18] and for L0 on a rutile single crystal through angle resolved XPS where the surface sensitivity is controlled by varying the emission angle.[21] Given this previous data, this depth effect is the most likely the origin of the 3:1 ratio of N environments, but without further depth profiling measurements, it is not possible to confirm if a proportion of the molecules are in the dissociated bidentate bonding geometry as discussed above, which would be consistent with seeing some C–OH signal in O 1*s*.

We also note the consistency between our N 1*s* spectrum with that of L0 deposited *in situ* onto TiO_2 (sublimation in ultra-high vacuum).[21] This indicates that we are not seeing any notable contamination from the acetonitrile solvent used when preparing the electrodes.

The C 1*s* spectrum is presented in Fig. 4(a), which has been fit with four peaks. As this spectrum represents a complex combination of many different bonding environments, calculated energies of the C 1*s* orbitals are shown in Fig. 4(b) where the carbon environments are binned into five groups (C_1 to C_5). These calculated energies help understand the shape of the experimental spectrum: we attribute the most intense component, C_a at 284.8 eV, to be dominated by photoemission from carbon–carbon environments in the phenylamine rings. The peak at 288.6 eV (C_d) is assigned to the carboxyl carbon atom in the carboxylic acid anchoring group (COOH). These two peaks are separated by 3.8 eV, which matches that of benzoic acid on TiO_2.[26] The shoulder to higher binding energy of the main phenyl peak, fitted with two peaks C_b and C_c, are therefore attributed to the remaining carbon environments: carbon bound to the amine nitrogen (in the triphenylamine moiety), the C ≡ N nitrile carbon and the double-bonded carbon environment in the backbone of the molecule. The intensity between ~290 and ~294 eV is attributed to shake-up processes.[41]

The peak positions and corresponding areas obtained from the curve fitting are listed in Table I, but caution is needed when interpreting them. First, the sample was prepared *ex situ* (and briefly exposed to air while being transferred into vacuum), so some carbon contamination is inevitable. In particular, this would likely affect the intensity of the C–C peak (C_a), but additionally, contaminants, such as CO, would be expected to form higher binding energy species. Second, the spectrum was decomposed using symmetric Voigt peaks to represent electrons with similar binding energies. This approximation does not account for small variations in binding energy as has been explored for triphenylamine where the binding energy of C 1*s* electrons varies with the position in the ring (distance from the central N atom).[42] Another spectral complication arises from final

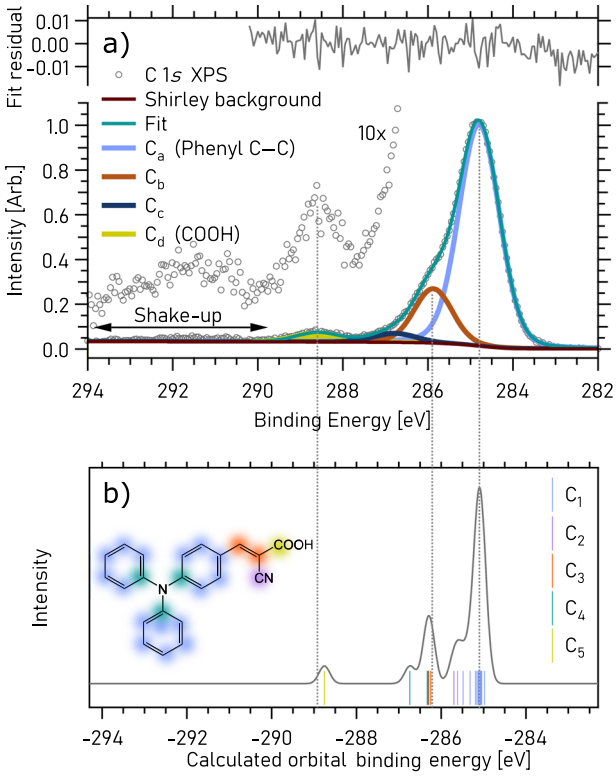

FIG. 4. (a) C 1*s* spectrum, measured with 600 eV photons, fitted with four components, each having Lorentzian and Gaussian widths of 0.2 eV and (1.0 ± 0.1) eV, respectively. (b) Colored vertical "sticks" indicate calculated C 1*s* orbital energies, shifted by 4.3 eV such that the HOMO orbital energy aligns with the experimental HOMO binding energy. The colors match the indicated carbon environments in the molecule scheme. The solid line shows a convolution of these orbital sticks with a Gaussian function (FWHM = 0.3 eV).

state effects. Given the optical absorption spectrum of the molecule on TiO_2,[43] with a maxima at 397 nm (3.2 eV), it is possible that there are shake-up excitations that overlap with the higher binding energy photoemission peaks. Finally, the effect of decreasing sensitivity of XPS with depth into the sample/molecule, discussed previously in

TABLE I. Summary of core-level binding energy (BE) positions, binding energy shifts (Δ) relative to the lowest binding energy peak, and normalized peak areas obtained from peak fitting of the XPS data ($h\nu$ = 600) eV.

		BE (eV)	Δ (eV)	Area
O 1*s*	Ti–O	530.05	···	0.56
	C = O/C–O–Ti	531.4	1.3	0.31
	C–OH	532.8	2.7	0.13
N 1*s*	$N_{nitrile}$	400.0	···	0.77
	N_{amine}	399.0	1.0	0.23
C 1*s*	C_a (phenyl)	284.8	···	0.76
	C_b	285.9	1.1	0.18
	C_c	286.8	2.0	0.03
	C_d (COOH)	288.6	3.8	0.03

relation to the relative intensities in N 1*s*, is also relevant for C 1*s* but to a lesser extent due to the increased photoelectron kinetic energy. For all of these reasons, the areas of the features are not expected to match the chemical structure particularly well.

We note that, without the supporting calculations, a temping assignment of C_c would be photoemission from C ≡ N as this peak has the same area as C_d (COOH). Not only is this inconsistent with the calculated energies but also it is inconsistent with XPS measurements of tetracyanoquinodimethane (TCNQ) where the binding energy separation between pyridine ring carbon and C ≡ N is reported to have values of 1.2[44] to 1.4 eV,[45] notably less than the 2 eV separation between C_a and C_c reported here.

A further complication with this sample is the presence of both COOH and COO^- species (evident in O 1*s* where only partial deprotonation is observed). In the study of L0 on rutile TiO_2(110), they attribute the feature at 286.5 eV to be COO^- species, which they infer from careful measurements of different surface coverages ranging from the sub-monolayer to multilayer.[21] The authors unfortunately do not discuss that why this binding energy is so low compared with monolayers of other de-protonated carboxylic acid based molecules on titania: aminobenzoic acid (288.4 eV),[46] various pyridine based molecules (288.8 eV),[26] and a bithiophene-carboxylic acid based molecule (288.5 eV).[47] On balance, the evidence in the current literature would suggest that the C_c feature in Fig. 4(a) does not originate from the carboxylic acid. This is supported by the calculated orbital energies [Fig. 4(b)], which imply that this feature may instead originate from other carbon atoms, specifically those bound to the triphenylamine nitrogen.

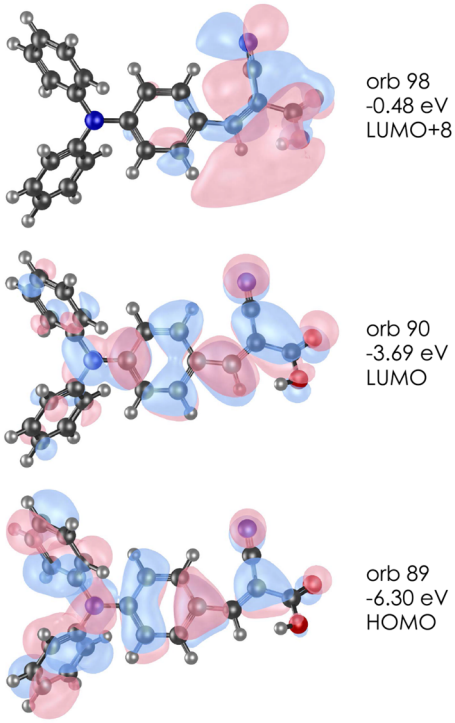

FIG. 5. Selected ground state molecular orbitals obtained from DFT. The LUMO and LUMO + 8 are dominantly responsible for the strongest N1*s* → π^* transitions in the TD-DFT ("A" and "B" resonances, respectively).

B. Electronic structure

Selected ground state molecular orbitals, relevant to the spectroscopy discussed below, are plotted in Fig. 5. These Kohn–Sham orbitals, of an isolated L0 molecule, provide a general picture of largely de-localized frontier orbitals with the HOMO and LUMO spanning the bridge between the acceptor and donor molecular components. Specifically, the HOMO (orbital 89) has higher density on the donating triphenylamine and the LUMO (orbital 90) has density skewed toward the cyanoacrylic acid, both with π/π^* lobes in the out-of-plane direction. The LUMO + 1 to LUMO + 7 (not plotted) all contribute to the delocalized out-of-plane π^* system distributed across the molecule. The LUMO + 8 (orbital 98) is the first virtual orbital with dramatically different character showing large in-plane lobes heavily localized on the cyanoacrylic acid. This matches the descriptions described elsewhere.[20]

Nitrogen 1*s* (K-edge) NEXAFS is included in Fig. 6 where the five experimentally distinct features are labeled A–E. This experimental spectrum is compared with a calculated spectrum, where TD-DFT was used to simulate the x-ray absorption process. This comparison helps deconstruct the NEXAFS in terms of transitions from the two N 1*s* atoms into the virtual/unoccupied molecular orbitals. A detailed breakdown of the transitions predicted by the TD-DFT can be found in the supplementary material.

The calculation predicts that the first excited state (A) originates from the nitrile N 1*s* to LUMO transition, and the second feature (B) is dominantly also from the nitrile N 1*s* to LUMO + 8 transition. Excitation from triphenylamine onto the LUMO is an incredibly weak resonance appearing as the third state in the calculation at ~401 eV. We note that the calculation places the initial state N 1*s* orbitals to have a separation of 1.7 eV (detailed in the supplementary material), notably larger than the 1.0 eV difference experimentally determined using XPS. Even taking this into consideration, the two LUMO resonances in the NEXAFS are separated

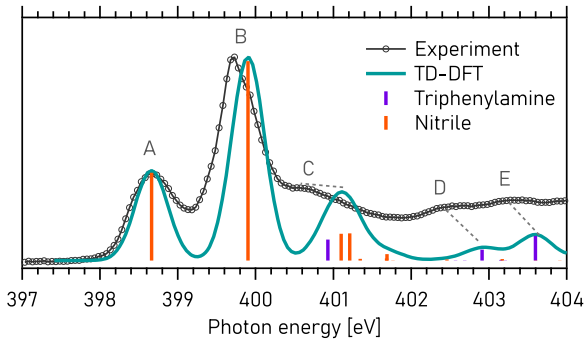

FIG. 6. Comparison between experimental NEXAFS and that simulated with TD-DFT. The calculated spectrum was obtained by convolving the oscillator strengths (shown with vertical sticks) with a Gaussian (0.5 eV FWHM). The contributions from the two nitrogen atoms are indicated. The full breakdown of the transitions is included in the supplementary material.

by more than the core-level splitting, implying that the core-hole influence is different in the two electron environments. However, regardless of the precise energy positioning of the two LUMO resonances, it is clear that the nitrile moiety is dominantly responsible for the overall NEXAFS intensity at lower photon energies (A–C). The calculation implies that the weaker, higher photon energy peaks D and E are predominantly transitions from triphenylamine.

Qualitatively, Fig. 6 shows a high level of consistency between the calculated and measured spectra, both in terms of the predicted shape and position of the main resonances. The above interpretation is largely consistent with previous experimental and computational analysis of the N 1*s* NEXAFS,[18,20] with the exception that this literature assigns resonance E to have contributions from both nitrogen atoms. This is potentially because our calculation focuses on the near-edge fine structure and is not designed to accurately model transitions into the higher energy diffuse/un-bound orbitals.

Figure 7(a) presents a "density of states" style plot, whereby the NEXAFS is presented on the same binding energy scale as the valence band XPS (measured at $h\nu$ = 220 eV). This is achieved by subtracting the N 1*s* core level binding energy from the photon energy scale of the N 1*s* (K-edge) NEXAFS. This alignment of occupied and unoccupied states is alike the method described elsewhere[48] where the energy definitions are described by the schematic in Fig. 7(b). For this molecule, the N 1*s* XPS (Fig. 3) shows two distinct N 1*s* orbitals, corresponding to atoms in the nitrile and triphenylamine moieties, with binding energies as detailed in Table I, both of which need to be considered. Figure 7(a) therefore shows two NEXAFS traces corresponding to the position of unoccupied states projected onto both the nitrile and amine nitrogen atoms. The binding energy positions of resonances A–E have been extracted from Fig. 7(a) and listed in Table II. The most appropriate trace in the DOS was selected for each transition based on the dominant intensity in the TD-DFT (Fig. 6): the nitrile projection for resonances A–C and the amine projection for D and E.

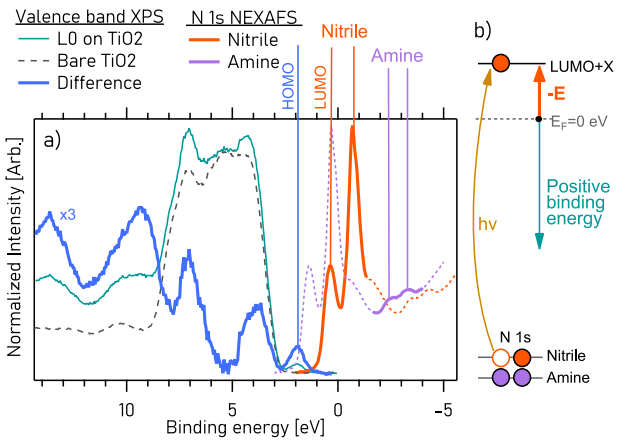

FIG. 7. (a) A "density of states" plot showing the valence band (XPS) and unoccupied states (N 1*s* NEXAFS) on the same binding energy axis. The two offset NEXAFS corresponding to projections of the same spectrum onto the nitrile and amine nitrogen atoms (see the text). The bold regions of the spectra correspond with features that dominantly originate from that atom. The difference spectrum is a subtraction of the bare electrode's valence band from the sensitized electrode highlighting the L0 features. (b) Scheme explaining how the binding energy scale is defined.

TABLE II. Energies of the five XAS features (A–E, as defined in Fig. 6) extracted from the DOS plot in Fig. 7 on the binding energy (BE) scale. In each case, the relevant projection was used. The energy relative to the HOMO (Δ) is also listed.

Feature	BE (eV)	Δ (eV)
HOMO	1.9	
A (LUMO)	0.35	1.5
B	−0.76	2.6
C	−1.7	3.5
D	−2.4	4.2
E	−3.3	5.1

It is of course worth remembering from the above discussion of the TD-DFT that the effect of the core-hole and surrounding electronic environments at the two nitrogen atoms may be different, so the relative positioning of the two projections in Fig. 7 may not be "correct." It is also worth highlighting that, while it is tempting to line up features in these two projections, for example, at ~0 eV, resonance A on the nitrile projection lines up with resonance B on the trimethylamine projection, and this can lead to incorrect conclusions. A purely experimental, and likely incorrect, conclusion from this may be that resonances A and B correspond to excitation from the two core levels into the same unoccupied orbital. However, as discussed above, this is not consistent with the literature[20] nor our TD-DFT calculation.

The conduction band edge of TiO_2 lies 3.0/3.2 eV above the valence band maximum for rutile/anatase.[49] In our data, the TiO_2 valence band maximum is at 2.9 eV binding energy (see the supplementary material), which places the conduction band edge at −0.2 ± 0.1 eV. Figure 7 therefore shows that the LUMO of the molecule lies below the conduction band edge in the core-excited state. Additionally, Fig. 7(a) also includes a difference spectrum, where the valence band of a bare TiO_2 electrode has been subtracted from that of the dye sensitized electrode highlighting the L0 features. The HOMO–LUMO gap in the core-excited state is 1.5 eV.

Figure 8(a) presents RPES measurements providing information about the occupied and unoccupied electronic states, including how these states couple and ultra-fast electron dynamics. Vertical line profiles have been extracted from the RPES map at binding energies intercepting the resonant Auger, at 15.8 eV binding energy, and the main participator enhancement at 7 eV. These have been plotted alongside the partial electron yield NEXAFS which, as expected, has a comparable shape to the line profile through the Auger. Each of the five main resonances, A–E, have a corresponding constant binding energy line profile plotted above the map. Figure 8(b) shows a type of "difference" map where the RPES has been divided by the shape of the off-resonance valence band. This processing is intended to highlight small differences in the spectral shape, but it is important to note that the intensities of features become meaningless. From this map, profiles through the participant region have been plotted in Fig. 8(c).

The RPES shows some participant enhancements of valence states, mainly on the A–C resonances at 0–6 eV binding energy. The

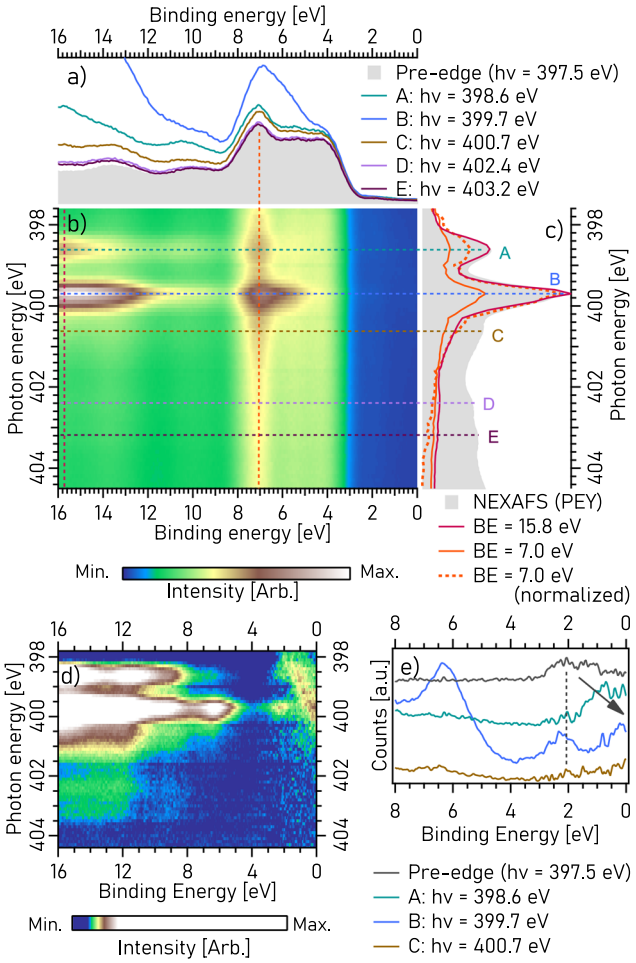

FIG. 8. N 1*s* (K-edge) RPES. (a) RPES measured on key resonances and off-resonance (pre-edge). (b) RPES map of the valence band as a function of photon energy. (c) NEXAFS where pink and orange lines show vertical line profiles extracted from the map through the Auger region (BE = 15.8 eV) and main participant region (7 eV), respectively. This is compared to partial electron yield (PEY) NEXAFS, which is normalized to the intensity of resonance "B." (d) An RPES "difference" map where the raw RPES is divided by the shape of the off-resonant valence band. (e) Line profiles extracted from the "difference" map. The vertical dashed line shows the position of the HOMO, and the diagonal arrow shows the second order N 1s photoemission.

map shows no visible enhancement on the TPA dominated resonances (D and E). Integrating the intensity of the participant region (between 5.5 and 7.5 eV) and comparing to that of the Auger region (15.5–16.0 eV), when the spectra are normalized to the B resonance, we observe a reduction in the intensity of resonance A. This suppression of participant decay at resonance A is attributed to electron de-localization from the nitrile nitrogen atom. This de-localization must be a result of an internal charge re-arrangement rather than charge transfer to the surface as the presence of the core-hole pulls the LUMO below the conduction band edge of the titania. This type of detailed RPES analysis can be found in the literature for both the *ex situ* prepared electrodes[20] and *in situ* single crystal study.[21] In the latter study, through controlling the polarization of the incoming radiation, the authors are able to much more clearly resolve resonances attributed to the electron donating TPA ("C" and "D" in Fig. 8) and used a core-hole-clock interpretation of resonant photoemission to infer an upper bound of 1.8 fs for the delocalization time-scale from the TPA. We will not further discuss the electron dynamics and instead point the readers to this literature.[20,21]

It is surprising that any participant enhancement of the HOMO is incredibly weak. At resonance B, we do see a very weak enhancement of the HOMO [visible only in the divided spectra in Figs. 8(d) and 8(e)]. The low intensity of this is perhaps not surprising as the π derived HOMO at the nitrile group has a nodal structure that extends perpendicularly from the plane of the molecule, whereas for the LUMO + 8, it lies in-plane (again consistent with past calculations[20]). However, the complete lack of orbital coupling between the HOMO and LUMO is surprising considering that these frontier orbitals (Fig. 5) show a very similar nodal structure on the nitrile part of the molecule.

IV. SUMMARY AND OUTLOOK

This paper presented a thorough photoelectron spectroscopy analysis of an mesoporous titania electrode sensitized with a triphenylamine-cyanoacrylic acid sensitizer. We discussed the O 1*s* and N 1*s* core level spectrum in the context of the different possible bonding geometries, while the C 1*s* spectrum was interpreted with the help of calculated C 1*s* orbital energies. The electronic structure, including both occupied and unoccupied frontier orbitals, was analyzed using valence band spectroscopy and x-ray absorption measurements providing insight into the energy alignment of states belonging to the acceptor (cyanoacrylic acid) and donor (triphenylamine) halves of the molecule. Time dependent density functional theory calculations showed that the N 1*s* X-ray absorption spectroscopy (XAS) is dominated by the nitrile moiety. Results show the LUMO, localized on the nitrile moiety, lies below the conduction band edge of the titania in the core-excited state and additionally provide evidence of electron de-localization away from the nitrile moiety within the core-hole lifetime. This resonant photoelectron spectroscopy data also revealed surprisingly weak coupling between the HOMO and the LUMO.

Throughout, we compared our measurements with existing literature on the same and related molecules, allowing this paper to act as a focused review on the topic while also providing critical validation though independent repeat measurements and calculations. The measurements and analysis presented here is overwhelmingly consistent with this existing literature, both in terms of the measurement and interpretation.[18–21] Repeat measurements of these kinds are surprisingly rare, but their value as part of the scientific method cannot be understated, especially in the context of attempting to build a body of work on their foundation.

This study aimed to provide a stepping stone toward measurements of flagship triphenylamine based dye sensitized photoelectrodes, which are substantially larger and more chemically complex than the molecule presented here. This work highlights that such future work needs a robust combination of theory and experiment and also the added value that tender or hard x-ray photoelectron spectroscopy would provide. Even the relatively small

molecule presented here provides notable challenges with the interpretation of the core-level spectra due to the combination of a complex mesoporous surface with the attenuation of the signal through the depth of the molecule. Disentangling these effects will get prohibitively harder as the molecules get larger making "bulk" sensitive measurements, using tender/hard X rays, a necessity.

SUPPLEMENTARY MATERIAL

See the supplementary material for the following: XPS measurements of a bare TiO_2 electrode; spectra comparing bare and sensitized electrodes; spectra of different samples showing reproducible sample preparation; NEXAFS spectroscopy study of x-ray beam induced radiation damage; comparison of partial and total electron yield NEXAFS; method for determining the valance band maximum position of a bare TiO_2 electrode; and output of the TD-DFT calculation detailing the excited states and electronic transitions.

ACKNOWLEDGMENTS

We acknowledge MAX IV Laboratory for time on beamline FlexPES under Proposal No. 20190866. Research conducted at MAX IV, a Swedish national user facility, is supported by the Swedish Research council under Contract No. 2018-07152, the Swedish Governmental Agency for Innovation Systems under Contract No. 2018-04969, and Formas under Contract No. 2019-02496. We are also grateful for travel support through the CALIPSOplus program (EU Horizon 2020 Grant No. 730872).

This work was supported by the UK Engineering and Physical Sciences Research Council (EPSRC) through the Overseas Travel Grant (OTG; Grant No. EP/T004355/1) and the EPSRC Fuel Cells and their Fuels Centre for Doctoral Training (CDT). We also acknowledge the University of Nottingham Propulsion Futures Beacon and Innovate UK through the Energy Research Accelerator (ERA) for funding toward this research. R.H.T. also acknowledges postdoc funding from both Nottingham University and Lund University.

DATA AVAILABILITY

The data that support the findings of this study are available from the corresponding authors upon reasonable request.

REFERENCES

[1]S. Yun, N. Vlachopoulos, A. Qurashi, S. Ahmad, and A. Hagfeldt, Chem. Soc. Rev. **48**, 3705 (2019).
[2]P. Bi and X. Hao, Sol. RRL **3**, 1970011 (2019).
[3]K. Sharma, V. Sharma, and S. S. Sharma, Nanoscale Res. Lett. **13**, 381 (2018).
[4]C. S. Ponseca, P. Chábera, J. Uhlig, P. Persson, and V. Sundström, Chem. Rev. **117**, 10940 (2017).
[5]N. Kaur, M. Singh, D. Pathak, T. Wagner, and J. M. Nunzi, Synth. Met. **190**, 20 (2014).
[6]M. Grätzel, J. Photochem. Photobiol., C **4**, 145 (2003).
[7]B. O'Regan and M. Grätzel, Nature **353**, 737 (1991).
[8]J. H. Yum, T. W. Holcombe, Y. Kim, K. Rakstys, T. Moehl, J. Teuscher, J. H. Delcamp, M. K. Nazeeruddin, and M. Grätzel, Sci. Rep. **3**, 2446 (2013).
[9]Y. Hao, Y. Saygili, J. Cong, A. Eriksson, W. Yang, J. Zhang, E. Polanski, K. Nonomura, S. M. Zakeeruddin, M. Grätzel, A. Hagfeldt, and G. Boschloo, ACS Appl. Mater. Interfaces **8**, 32797 (2016).
[10]J. Zhang, N. Vlachopoulos, Y. Hao, T. W. Holcombe, G. Boschloo, E. M. J. Johansson, M. Grätzel, and A. Hagfeldt, ChemPhysChem **17**, 1441 (2016).
[11]Y. Farré, M. Raissi, A. Fihey, Y. Pellegrin, E. Blart, D. Jacquemin, and F. Odobel, ChemSusChem **10**, 2618 (2017).
[12]Y. Ren, D. Sun, Y. Cao, H. N. Tsao, Y. Yuan, S. M. Zakeeruddin, P. Wang, and M. Grätzel, J. Am. Chem. Soc. **140**, 2405 (2018).
[13]R. H. Temperton, S. T. Skowron, A. Gibson, K. Handrup, and J. N. O'Shea, Chem. Phys. Lett. **747**, 137309 (2020).
[14]R. H. Temperton, N. W. Rosemann, M. Guo, N. Johansson, L. A. Fredin, O. Prakash, K. Wärnmark, K. Handrup, J. Uhlig, J. Schnadt, and P. Persson, J. Phys. Chem. A **124**, 1603 (2020).
[15]A. J. Gibson, R. H. Temperton, K. Handrup, M. Weston, L. C. Mayor, and J. N. O'Shea, J. Chem. Phys. **140**, 234708 (2014).
[16]L. C. Mayor, J. Ben Taylor, G. Magnano, A. Rienzo, C. J. Satterley, J. N. O'Shea, and J. Schnadt, J. Chem. Phys. **129**, 114701 (2008).
[17]R. H. Temperton, S. T. Skowron, K. Handrup, A. J. Gibson, A. Nicolaou, N. Jaouen, E. Besley, and J. N. O'Shea, J. Chem. Phys. **151**, 074701 (2019).
[18]E. M. J. Johansson, T. Edvinsson, M. Odelius, D. P. Hagberg, L. Sun, A. Hagfeldt, H. Siegbahn, and H. Rensmo, J. Phys. Chem. C **111**, 8580 (2007).
[19]M. Hahlin, E. M. J. Johansson, S. Plogmaker, M. Odelius, D. P. Hagberg, L. Sun, H. Siegbahn, and H. Rensmo, Phys. Chem. Chem. Phys. **12**, 1507 (2010).
[20]M. Hahlin, M. Odelius, M. Magnuson, E. M. J. Johansson, S. Plogmaker, D. P. Hagberg, L. Sun, H. Siegbahn, and H. Rensmo, Phys. Chem. Chem. Phys. **13**, 3534 (2011).
[21]S. Yu, S. Ahmadi, M. Zuleta, H. Tian, K. Schulte, A. Pietzsch, F. Hennies, J. Weissenrieder, X. Yang, and M. Göthelid, J. Chem. Phys. **133**, 224704 (2010).
[22]M. Pastore and F. De Angelis, Phys. Chem. Chem. Phys. **14**, 920 (2012).
[23]C. Anselmi, E. Mosconi, M. Pastore, E. Ronca, and F. De Angelis, Phys. Chem. Chem. Phys. **14**, 15963 (2012).
[24]E. L. Unger, T. Edvinsson, J. D. Roy-Mayhew, H. Rensmo, A. Hagfeldt, E. M. J. Johansson, and G. Boschloo, J. Phys. Chem. C **116**, 21148 (2012).
[25]S. K. Eriksson, I. Josefsson, H. Ellis, A. Amat, M. Pastore, J. Oscarsson, R. Lindblad, A. I. K. Eriksson, E. M. J. Johansson, G. Boschloo, A. Hagfeldt, S. Fantacci, M. Odelius, and H. Rensmo, Phys. Chem. Chem. Phys. **18**, 252 (2016).
[26]J. Schnadt, J. N. O'Shea, L. Patthey, J. Schiessling, J. Krempaský, M. Shi, N. Mårtensson, and P. a. Brühwiler, Surf. Sci. **544**, 74 (2003).
[27]Y. Shao, Z. Gan, E. Epifanovsky, A. T. B. Gilbert, M. Wormit, J. Kussmann, A. W. Lange, A. Behn, J. Deng, X. Feng, D. Ghosh, M. Goldey, P. R. Horn, L. D. Jacobson, I. Kaliman, R. Z. Khaliullin, T. Kuś, A. Landau, J. Liu, E. I. Proynov, Y. M. Rhee, R. M. Richard, M. A. Rohrdanz, R. P. Steele, E. J. Sundstrom, H. L. Woodcock, P. M. Zimmerman, D. Zuev, B. Albrecht, E. Alguire, B. Austin, G. J. O. Beran, Y. A. Bernard, E. Berquist, K. Brandhorst, K. B. Bravaya, S. T. Brown, D. Casanova, C.-M. Chang, Y. Chen, S. H. Chien, K. D. Closser, D. L. Crittenden, M. Diedenhofen, R. A. DiStasio, H. Do, A. D. Dutoi, R. G. Edgar, S. Fatehi, L. Fusti-Molnar, A. Ghysels, A. Golubeva-Zadorozhnaya, J. Gomes, M. W. D. Hanson-Heine, P. H. P. Harbach, A. W. Hauser, E. G. Hohenstein, Z. C. Holden, T.-C. Jagau, H. Ji, B. Kaduk, K. Khistyaev, J. Kim, J. Kim, R. A. King, P. Klunzinger, D. Kosenkov, T. Kowalczyk, C. M. Krauter, K. U. Lao, A. D. Laurent, K. V. Lawler, S. V. Levchenko, C. Y. Lin, F. Liu, E. Livshits, R. C. Lochan, A. Luenser, P. Manohar, S. F. Manzer, S.-P. Mao, N. Mardirossian, A. V. Marenich, S. A. Maurer, N. J. Mayhall, E. Neuscamman, C. M. Oana, R. Olivares-Amaya, D. P. O'Neill, J. A. Parkhill, T. M. Perrine, R. Peverati, A. Prociuk, D. R. Rehn, E. Rosta, N. J. Russ, S. M. Sharada, S. Sharma, D. W. Small, A. Sodt, T. Stein, D. Stück, Y.-C. Su, A. J. W. Thom, T. Tsuchimochi, V. Vanovschi, L. Vogt, O. Vydrov, T. Wang, M. A. Watson, J. Wenzel, A. White, C. F. Williams, J. Yang, S. Yeganeh, S. R. Yost, Z.-Q. You, I. Y. Zhang, X. Zhang, Y. Zhao, B. R. Brooks, G. K. L. Chan, D. M. Chipman, C. J. Cramer, W. A. Goddard, M. S. Gordon, W. J. Hehre, A. Klamt, H. F. Schaefer, M. W. Schmidt, C. D. Sherrill, D. G. Truhlar, A. Warshel, X. Xu, A. Aspuru-Guzik, R. Baer, A. T. Bell, N. A. Besley, J.-D. Chai, A. Dreuw, B. D. Dunietz, T. R. Furlani, S. R. Gwaltney, C.-P. Hsu, Y. Jung, J. Kong, D. S.

Lambrecht, W. Liang, C. Ochsenfeld, V. A. Rassolov, L. V. Slipchenko, J. E. Subotnik, T. Van Voorhis, J. M. Herbert, A. I. Krylov, P. M. W. Gill, and M. Head-Gordon, Mol. Phys. **113**, 184 (2015).
[28]A. D. Becke, J. Chem. Phys. **98**, 5648 (1993).
[29]P. J. Stephens, F. J. Devlin, C. F. Chabalowski, and M. J. Frisch, J. Phys. Chem. **98**, 11623 (1994).
[30]B. P. Pritchard, D. Altarawy, B. Didier, T. D. Gibson, and T. L. Windus, J. Chem. Inf. Model. **59**, 4814 (2019).
[31]N. A. Besley, M. J. G. Peach, and D. J. Tozer, Phys. Chem. Chem. Phys. **11**, 10350 (2009).
[32]A. Gilbert, IQmol, 2020.
[33]F. Viñes, C. Sousa, and F. Illas, Phys. Chem. Chem. Phys. **20**, 8403 (2018).
[34]R. Temperton, A. Gibson, K. Handrup, and J. O'Shea, J. Chem. Phys. **147**, 054703 (2017).
[35]L. Patthey, H. Rensmo, P. Persson, K. Westermark, L. Vayssieres, A. Stashans, Å. Petersson, P. A. Brühwiler, H. Siegbahn, S. Lunell, and N. Mårtensson, J. Chem. Phys. **110**, 5913 (1999).
[36]A. G. Thomas and K. L. Syres, Chem. Soc. Rev. **41**, 4207 (2012).
[37]P. Persson and S. Lunell, Sol. Energy Mater. Sol. Cells **63**, 139 (2000).
[38]J. G. Ma, C. R. Zhang, J. J. Gong, B. Yang, H. M. Zhang, W. Wang, Y. Z. Wu, Y. H. Chen, and H. S. Chen, J. Chem. Phys. **141**, 234705 (2014).
[39]M. H. Ahmed, R. H. Temperton, and J. N. O'Shea, "An in situ exploration of subsurface defect migration to a liquid water-exposed rutile TiO_2(110) surface by XPS," Surf. Interface Anal. (published online).
[40]W. J. Gammon, O. Kraft, A. C. Reilly, and B. C. Holloway, Carbon **41**, 1917 (2003).
[41]C. Enkvist, S. Lunell, B. Sjögren, S. Svensson, P. A. Brühwiler, A. Nilsson, A. J. Maxwell, and N. Mårtensson, Phys. Rev. B **48**, 14629 (1993).
[42]T. Zhang, I. E. Brumboiu, C. Grazioli, A. Guarnaccio, M. Coreno, M. de Simone, A. Santagata, H. Rensmo, B. Brena, V. Lanzilotto, and C. Puglia, J. Phys. Chem. C **122**, 17706 (2018).
[43]D. P. Hagberg, T. Marinado, K. M. Karlsson, K. Nonomura, P. Qin, G. Boschloo, T. Brinck, A. Hagfeldt, and L. Sun, J. Org. Chem. **72**, 9550 (2007).
[44]M. J. Capitán, J. Álvarez, and C. Navio, Phys. Chem. Chem. Phys. **20**, 10450 (2018).
[45]R. Precht, R. Hausbrand, and W. Jaegermann, Phys. Chem. Chem. Phys. **17**, 6588 (2015).
[46]A. G. Thomas, M. J. Jackman, M. Wagstaffe, H. Radtke, K. Syres, J. Adell, A. Lévy, and N. Martsinovich, Langmuir **30**, 12306 (2014).
[47]J. Dervaux, P.-A. Cormier, C. Struzzi, M. Scardamaglia, C. Bittencourt, L. Petaccia, D. Cornil, L. Lasser, D. Beljonne, J. Cornil, R. Lazzaroni, and R. Snyders, J. Chem. Phys. **147**, 244704 (2017).
[48]J. Schnadt, J. N. O'Shea, L. Patthey, J. Krempaský, N. Mårtensson, and P. A. Brühwiler, Phys. Rev. B **67**, 235420 (2003).
[49]D. O. Scanlon, C. W. Dunnill, J. Buckeridge, S. A. Shevlin, A. J. Logsdail, S. M. Woodley, C. R. A. Catlow, M. J. Powell, R. G. Palgrave, I. P. Parkin, G. W. Watson, T. W. Keal, P. Sherwood, A. Walsh, and A. A. Sokol, Nat. Mater. **12**, 798 (2013).